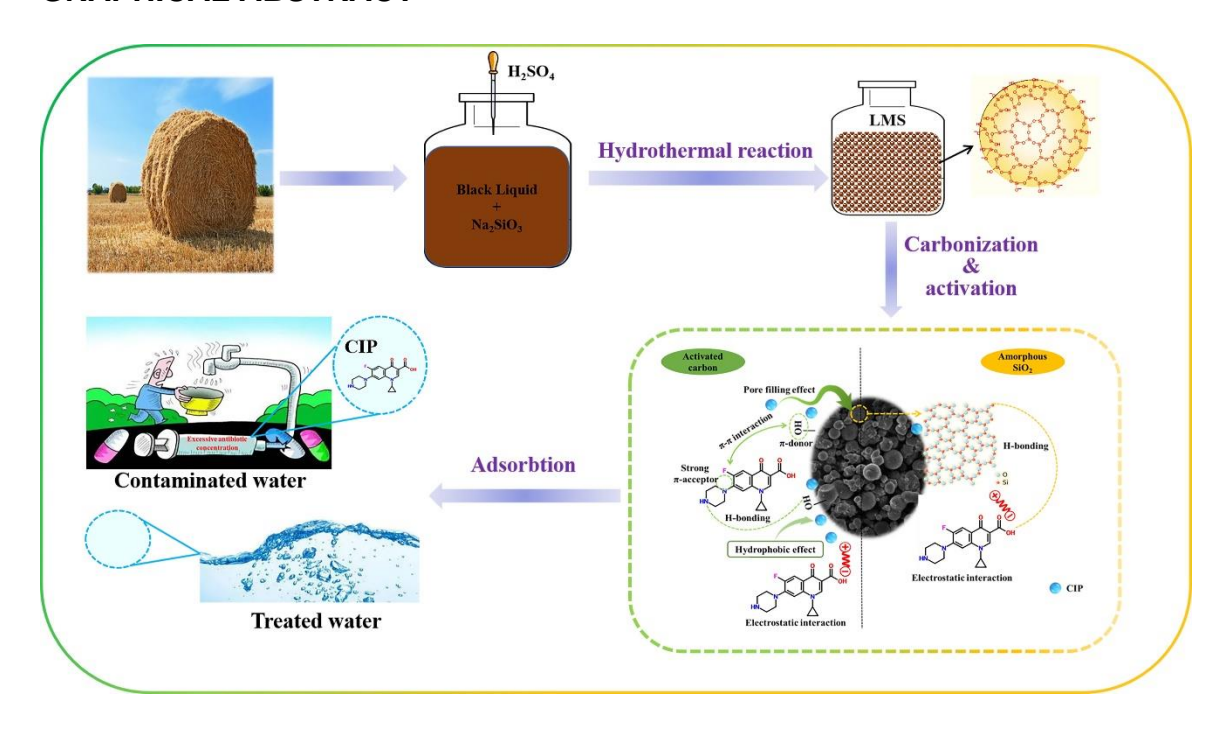
Role of Intrinsic and Extrinsic Silicon on the Structure and Adsorption Properties of Lignin-Based Spherical Porous Carbon

Shuangfeng Li, ^a Sen Yao, ^d Huai Wang, ^a Yong Sun, ^d Risheng Yao, ^{a,*} and Fenghe Li , ^{b,a,c,*}

* Corresponding author: lifenghe@ahmu.edu.cn; rishengyao@163.com

DOI: 10.15376/biores.20.2.4229-4249

GRAPHICAL ABSTRACT



Role of Intrinsic and Extrinsic Silicon on the Structure and Adsorption Properties of Lignin-Based Spherical Porous Carbon

Shuangfeng Li, ^a Sen Yao, ^d Huai Wang, ^a Yong Sun, ^d Risheng Yao, ^{a,*} and Fenghe Li , ^{b,a,c,*}

The influence of SiO_2 on the properties of lignin spherical porous carbon (LSC) was examined. Evidence suggested that the presence of optimal SiO_2 contributed to stabilizing the spherical structure of LSC and significantly enhanced LSC's ability to adsorb antibiotics. Lignin/ SiO_2 composite microspheres, fabricated through co-precipitation with added sodium silicate, served as precursors for C/SiO_2 composite microspheres (LSC- $Si^{(+)}$). LSC- $Si^{(+)}$ demonstrated excellent adsorption capacity for ciprofloxacin (CIP), sulfadiazine (SDZ), and tetracycline hydrochloride (TC). Furthermore, LSC- $Si^{(+)}$ exhibits excellent physicochemical stability and noteworthy recyclability, maintaining high adsorption capacity after five cycles of recycling. Given the benefits of low cost, ease of production, and excellent adsorption performance, LSC- $Si^{(+)}$ -20 holds promise for removing antibiotic contaminants from wastewater.

DOI: 10.15376/biores.20.2.4229-4249

Keywords: Lignin spherical porous carbon; Antibiotics; Wastewater treatment

Contact information: a: School of Food and Biological Engineering, Hefei University of Technology, Hefei, 2300601, China; b: School of Pharmacy, the Second Affiliated Hospital, University of Medicine, Hefei, 230032, China; c: Postdoctoral Workstation of Anhui Huaheng Biotechnology Co., Ltd. Hefei, 230061, China; d: Anhui Tongsu Technology Co., Ltd. Hefei, 230088, China; *Corresponding author: lifenghe@ahmu.edu.cn; rishengyao@163.com

INTRODUCTION

Carbon materials have become one of the most attractive materials in the 21st century (Balandin 2011). Among them, spherical porous carbon materials possess extremely high chemical and thermal stability, an adjustable specific surface area, pore structure, and surface chemistry, as well as regular spherical morphology and high adsorption capacity. These properties have led to their extensive application in water treatment (Ma *et al.* 2012; Han *et al.* 2000; Tran *et al.* 2020; Gao *et al.* 2021). In addition, their utilization extends to energy storage and conversion, catalysis, blood purification, air purification, and soil remediation (Sun and Li 2004; Kolb *et al.* 2017; Ouzzine *et al.* 2019; Wang 2019; Kameda *et al.* 2020; Wang *et al.* 2020; Xu *et al.* 2020).

However, precursors for spherical porous carbon materials primarily rely on petrochemicals and their derivatives, which exert significant pressure on the environment and energy resources (Liu *et al.* 2015). With the emergence of "green chemistry," the development of bio spherical porous carbon has captured global attention. Spherical lignin is considered an ideal carbon precursor due to its abundance of functional groups, consistent morphology, adjustable size, high aromatic ring content (up to 60% carbon), and renewable nature (Guo *et al.* 2017; Moreno and Sipponen 2020).

The preparation of spherical lignin-based porous carbon mainly includes two processes: carbonization and activation. First, carbonization treatment is conducted to convert spherical lignin, serving as the precursor, into carbon black with a high carbon content. Then, physical or chemical activation treatment is applied to develop the pore structure of the lignin-derived carbon black, thereby increasing its specific surface area and pore volume. In general, the larger the specific surface area and pore volume of spherical porous carbon, the stronger the adsorption capacity. But, it depends on the specific application.

For the preparation of spherical lignin porous carbon, the most important step is to prepare spherical lignin carbon precursors. The primary techniques for synthesizing the spherical lignin precursor include direct acid hydrolysis (Al-Lagtah et al. 2016; Liu et al. 2020), self-assembly (Zhao et al. 2016; Jiang 2019), crosslinking polymerization (Yu et al. 2018), spray drying (Liu et al. 2020), and hydrothermal treatment. Among these, hydrothermal treatment is preferred due to its simplicity, controllability, high efficiency, and environmental benefits. Using this method, Mao et al. (2018) produced lignin carbon spheres through hydrothermal carbonization, starting with enzymatically digested lignin as the raw material. Similarly, spherical lignin has been created by dissolving lignosulfonate in an acidic aqueous solution and applying hydrothermal treatment (Fan 2020; Fan et al. 2020). Ho et al. (2019) used a solvothermal reaction with dimethylsulfoxide as the solvent to prepare lignin carbon spheres. Pang et al. (2021) generated lignin microspheres by adding poly(vinylpyrrolidone) as a surfactant to a hydrothermal reaction involving kraft lignin. Notably, all previous studies have utilized either laboratory-extracted or commercially available lignin as precursors, synthesizing spherical lignin through solubilization and recombination of lignin molecules, necessitating the use of costly chemicals and specialized laboratory equipment. Additionally, spherical lignin can also be effectively prepared from black liquor (BL). Cha et al. (2020) successfully extracted lignin microspheres (LM) directly from the BL of Miscanthus sacchariflorus using controlled pH adjustments and hydrothermal treatment. These microspheres were characterized by their polydispersity, smooth surfaces, and narrow size distribution, making this method highly suitable for the direct and large-scale extraction of lignin microspheres from BL.

There are both lignin and silicates present in biomass black liquor. In the solution, silica functionalities are mainly surface silanol groups (SiOH); they can be protonated or deprotonated in water, and they can interact with polar groups or molecules via hydrogen bond interactions (Valetti *et al.* 2017). Lignin can form a reinforced three-dimensional network structure through electrostatic adsorption with SiO₂ in water (Valetti *et al.* 2017). SiO₂ exhibits excellent mechanical properties and thermal stability, and their derivatives are widely used to achieve the high-value use of lignin (Wang *et al.* 2021).

Antibiotics (ATs) are emerging contaminants frequently detected in the subsurface environment (López-Serna et al. 2013; Goldstein et al. 2014; Qiu et al. 2019; Ben et al. 2020). These compounds pose potential long-term health risks, even at low concentrations (Zhang et al. 2018; Zhang et al. 2019). Antibiotic residues in the environment can have adverse effects on both soil organisms (Thiele-Bruhn and Beck 2005) and plants (Reichel et al. 2015). Sorption is a crucial process that controls the mobility, fate, bioavailability, and reactivity of antibiotics in the environment (Zhang et al. 2013). Adsorption is recognized as the most promising and cost-effective method for removing various emerging contaminants from water and wastewater bodies (Sophia et al. 2018).

When preparing LSC with wheat straw BL using a hydrothermal treatment-carbonization-activation method, the authors observed differences in morphology and ciprofloxacin (CIP) adsorption capacity between LSC derived from primary and desilicated BL; notably, the structure of LM was more regular and smoother than that of LM-Si(-), exhibiting better dispersion. At the same time, during carbonization and activation, the structure of LSC-Si(-) was being more severely compromised. In addition, the adsorption capacity from desilicated BL was lower. Therefore, this paper aimed to analyze the impact of SiO₂ on the structure and adsorption capacity of lignin spherical porous carbon, and to introduce new methods for preparing high-performance C/SiO₂ composite microspheres from sodium silicate-enhanced BL.

EXPERIMENTAL

Materials

Wheat straw was obtained from Changfeng County, Hefei City, Anhui province. Ciprofloxacin (CIP), tetracycline hydrochloride (TC), sulfadiazine (SDZ), potassium dichromate (Cr⁶⁺), Na₂SiO₃•9H₂O, sodium hydroxide (NaOH), and potassium hydroxide (KOH) were purchased from Shanghai Aladdin Biochemical Technology Co., LTD. Sulfuric acid (H₂SO₄), hydrofluoric acid (HF), and hydrochloric acid (HCl) were purchased from Sinopharm Holding Chemical Reagent Co., LTD. Chemicals were of analytical grade.

Preparation of Lignin Spherical Porous Carbon

To explore the impact of SiO₂ on the properties of lignin porous carbon, two types of lignin porous carbon were synthesized: The first type was desilicated lignin spherical porous carbon (LSC-Si⁽⁻⁾). 1% (w/v) calcium oxide was added to the BL, reacting at 25 °C for 1 h, followed by filtering to remove silica. The BL pH was adjusted to 1 through the dropwise addition of 72% H₂SO₄, followed by a hydrothermal reaction at 121 °C for 1 h. After the reaction, the mixture was cooled, filtered, and washed with deionized water under vacuum filtration until the pH of the permeate approximated 7, yielding lignin microspheres (LM-Si⁽⁻⁾). The prepared LM were carbonized at 700 °C and subsequently activated with KOH in a 1:2 mass ratio in a tubular furnace at 800 °C for 120 min under a nitrogen atmosphere. The mixture was then washed with hydrochloric acid to remove impurities, followed by a rinse with deionized water under vacuum filtration until the pH of the permeate approximated 7. Finally, the material was dried at 100 °C for 12 h to yield LSC-Si⁽⁻⁾. The second type was lignin spherical porous carbon (LSC). Primary BL served as the raw material, with all steps identical to those above, except that the desilication step was omitted to produce LSC.

Preparation of Silicon-modified Lignin Spherical Porous Carbon by Co-precipitation Method

To verify whether the artificially added silicon element can be successfully loaded onto LSC, Na₂SiO₃·9H₂O was selected as the Si source. Na₂SiO₃·9H₂O was added to BL at 10 g/L and stirred at 60 $^{\circ}$ C for 1 h. The hydrothermal reaction, carbonization and activation processes were the same as the preparation of lignin spherical porous carbon described above, and the sample was named LSC-Si⁽⁺⁾-10.

Effect of Different Silica Contents on the Properties of LSC-Si(+)

 $Na_2SiO_3 \cdot 9H_2O$ was added to the BL according to the addition amount of 5-25 g/L and stirred at 60 °C for 1 h. The hydrothermal reaction, carbonization and activation processes were the same as the preparation of lignin spherical porous carbon described above, and LSC-Si⁽⁺⁾ with different SiO₂ content is prepared. According to the amount of $Na_2SiO_3 \cdot 9H_2O$ added, they were named as LSC-Si⁽⁺⁾-5, LSC-Si⁽⁺⁾-10, LSC-Si⁽⁺⁾-20, LSC-Si⁽⁺⁾-25.

To verify the effect of the presence of SiO₂ on the performance of LSC-Si⁽⁺⁾, 30% HF was used to react at 80 °C, 150 rpm for 4 h to remove SiO₂. During the experiment, the container is opened in a fume hood.

Characterization

The surface morphology and composition of samples were examined with the help of a scanning electron microscope (SEM, Gemini 500, Carl Zeiss, Germany). X-ray photoelectron spectroscopy (XPS, Thermo Nicolet, USA) analysis was made with the help of Thermo Scientific KAlpha determining the chemical-structure of porous carbon. The structural confirmation was made with the help of Fourier-transform infrared (FTIR) spectroscopy.

The measurements were obtained using a Nicolet 6700 spectrometer (Thermo Nicolet, USA) with a 4 cm⁻¹ resolution in the range of 4000 to 600 cm⁻¹. Brunauer-Emmett-Teller (BET) surface area, pore size, and total pore volume were obtained using a specific surface area and aperture analyzer (Micromeritics ASAP 2460, USA).

Antibiotics concentrations were measured using an ultraviolet spectrophotometer (UV-117A, Agilent, USA). In order to obtain more structural information of the materials, X-ray diffraction (XRD) characterization was performed (PAN analytical X-Pert PRO MPD, Netherlands).

Antibiotic Adsorption Selectivity of LSC-Si⁽⁺⁾-20

The adsorption capacity of LSC-Si⁽⁺⁾-20 on CIP, sulfadiazine (SDZ) and tetracycline hydrochloride (TC) was investigated: 10 mg of LSC-Si⁽⁺⁾-20 was mixed with 40 mL of antibiotic solution at a concentration of 200 mg/L, and LSC was used as a control. The adsorption test was carried out at 25 °C until the adsorption equilibrium, and the supernatant was filtered through 0.22 μ m filter membrane. The concentration was determined by UV spectrophotometer.

Adsorption of Heavy Metal Ions Cr (VI)

In order to explore the adsorption capacity of LSC-Si⁽⁺⁾-20 on heavy metal ions, it was applied to the adsorption of Cr⁶⁺. 10 mg of LSC-Si⁽⁺⁾-20 was mixed with 60 mL of Cr⁶⁺ at a concentration of 100 mg/L, and LSC was used as a control. The adsorption test was carried out at 25 °C until the adsorption equilibrium, and the supernatant was filtered through 0.22 μ m filter membrane.

The concentration of Cr⁶⁺ before and after adsorption was determined by dibenzoyl dihydrazine spectrophotometry at 540 nm.

Batch Adsorption Experiments

In experiments of equilibrium adsorption isotherm, LSC-Si⁽⁻⁾, LSC, LSC-Si⁽⁺⁾-5, LSC-Si⁽⁺⁾-10, LSC-Si⁽⁺⁾-20, LSC-Si⁽⁺⁾-25 (10 mg) and CIP solution (C₀=50-300 mg/L, 80 mL) were placed in a 250 mL Erlenmeyer flask and shaken for 12 h by an incubator at the constant temperature of 298 K. In kinetic adsorption tests, the absorption was measured at different time intervals (1-360 min) after 200 mL of CIP solution (100 mg/L) at 298 K was mixed with 50 mg LSC-Si⁽⁻⁾, LSC, LSC-Si⁽⁺⁾-5, LSC-Si⁽⁺⁾-10, and LSC-Si⁽⁺⁾-20, respectively.

Adsorption thermodynamic tests were carried out using an adsorbent of 10 mg (LSC and LSC-Si⁽⁺⁾-5) and CIP solution (40 mL) comprising 150 mg/L at temperatures ranging from 298 to 318 K. Following the adsorption, the obtained mixture was filtered with the help of syringe filter (0.22 µm). Afterwards, the residual CIP solution concentration was determined using a UV–vis spectrophotometer at a specific wavelength of 278 nm. All of the adsorption tests were conducted in triplicate, and their average value was determined.

Equation 1 was used to calculate the adsorption capacity of the prepared adsorbent,

$$Q_e = \frac{(C_0 - C_t) \times V}{W} \tag{1}$$

where Q_e (mg/g), C_0 (mg/L), C_t (mg/L), V (L), and W (mg) values represent the adsorption capacity at time t (min), initial CIP concentration, residual CIP concentration at t, volume of solution, and mass of the adsorbent, respectively.

The Langmuir (Eq. 2) and Freundlich (Eq. 3) isotherm models and separation factor (Eq. 4) are presented as follows,

$$Q_e = \frac{Q_{max} K_L C_e}{1 + K_L C_e} \tag{2}$$

$$Q_e = K_F C_e^{1/n} \tag{3}$$

$$R_L = \frac{1}{1 + K_L \, C_0} \tag{4}$$

where Q_e (mg/g), Q_{max} (mg/g), C_e (mg/L), K_L and K_F (L/mg), and n stand for the equilibrium adsorption capacity (mg/g), the maximum adsorption capacity, the equilibrium concentration, the Langmuir constants, and Freundlich constants indicating the adsorption capacity as well as intensity, respectively.

Equations 5 and 6 represent the pseudo-first-order, and pseudo-second-order kinetic models,

$$Q_t = Q_e(1 - e^{-k_1 t}) (5)$$

$$Q_{\rm t} = \frac{k_2 Q_{\rm e}^2 t}{1 + k_2 Q_{\rm e} t} \tag{6}$$

where k_1 and k_2 are the adsorption rate constant (L/min) and the rate constant (g/mg·min), respectively.

The intraparticle diffusion model (Eq. 7) is described as follows,

$$Q_t = K_i t^{0.5} + C_i (7)$$

where k_i is the rate constant (mg/g·min0.5) and C_i is the intercept relating to the boundary layer thickness.

The thermal changes during the adsorption process were assessed using thermodynamic parameters. In this regard, the Gibbs energy change (ΔG° , kJ/mol) is represented by Eq. 8, while the enthalpy change (ΔH° , kJ/mol) and entropy change (ΔS° , J/mol•K) were calculated by Eqs. 9 through 11 (Lima *et al.* 2019),

$$\Delta G^{\circ} = \Delta H^{\circ} - T\Delta S^{\circ} \tag{8}$$

$$\Delta G^{\circ} = -RT ln K_C \tag{9}$$

$$K_C = \frac{Q_e}{C_e} K \tag{10}$$

$$ln\frac{c_{Ac}}{c_e} = -\frac{\Delta H^{\circ}}{RT} + \frac{\Delta S^{\circ}}{R} \tag{11}$$

where K_c is the equilibrium constant. R (8.314 J/K•mol) represents the universal gas constant, while the T (K) indicates the absolute temperature.

Regeneration Performance of LSC-Si⁽⁺⁾-20

The recoverability of the adsorbent is very important for practical applications (Hou *et al.* 2021). Since the solution recovery method consumes a large amount of solvents and improper treatment can easily lead to secondary pollution of water resources by acidity or alkalinity, the pyrolysis method was used to recover LSC-Si⁽⁺⁾-20, the specific operation is: the adsorbed porous carbon was heated to 700 °C at a rate of 10 °C/min under an N_2 atmosphere and pyrolyzed at this constant temperature for 60 min.

RESULTS AND DISCUSSION

Effect of SiO₂ on the Properties of Lignin Spherical Porous Carbon

Si-O-C represents the characteristic peak of SiO₂. As shown in Fig 1a, the Si-O-C peak in LSC-Si⁽⁻⁾ was notably weaker compared to that in LSC, indicating significant removal of SiO₂.

As indicated in Fig. 1 (b), LSC demonstrated superior adsorption capacity for CIP compared to LSC-Si⁽⁻⁾. It is evident that the presence of SiO₂ enhanced the adsorption capacity of LSC for CIP. Comparison of the SEM images in Fig 1 (c) and (e) reveals that the structure of LM was more regular and smoother than that of LM-Si⁽⁻⁾, exhibiting better dispersion. From Figs. 1 (d) and (f), it was observed that the spherical structures of both LSC and LSC-Si⁽⁻⁾ exhibited varying degrees of fusion and collapse, with the structure of LSC-Si⁽⁻⁾ being more severely compromised.

SiO₂ enhanced the adsorption capacity of CIP by LSC. The primary reason may be that SiO₂ forms hydrogen bonds with lignin and adheres to the surface of LSC (Zhong *et al.* 2015). Due to the polar nature of the Si-O bond, Si-O-C groups exhibit distinct charge distribution, facilitating the adsorption of CIP by LSC. Simultaneously, SiO₂ in solution forms hydrogen-bonded adsorption with CIP, demonstrating significant adsorption capacity for CIP (Valetti *et al.* 2017). A second reason might be that lignin, with its low thermal decomposition temperature, is susceptible to collapse during high-temperature pyrolysis, while SiO₂, possessing robust substrate strength and mechanical stress resistance, serves as a hard template agent supporting the lignin carbon skeleton. This prevents aggregation and collapse of LSC, thus enhancing its spherical structural stability.

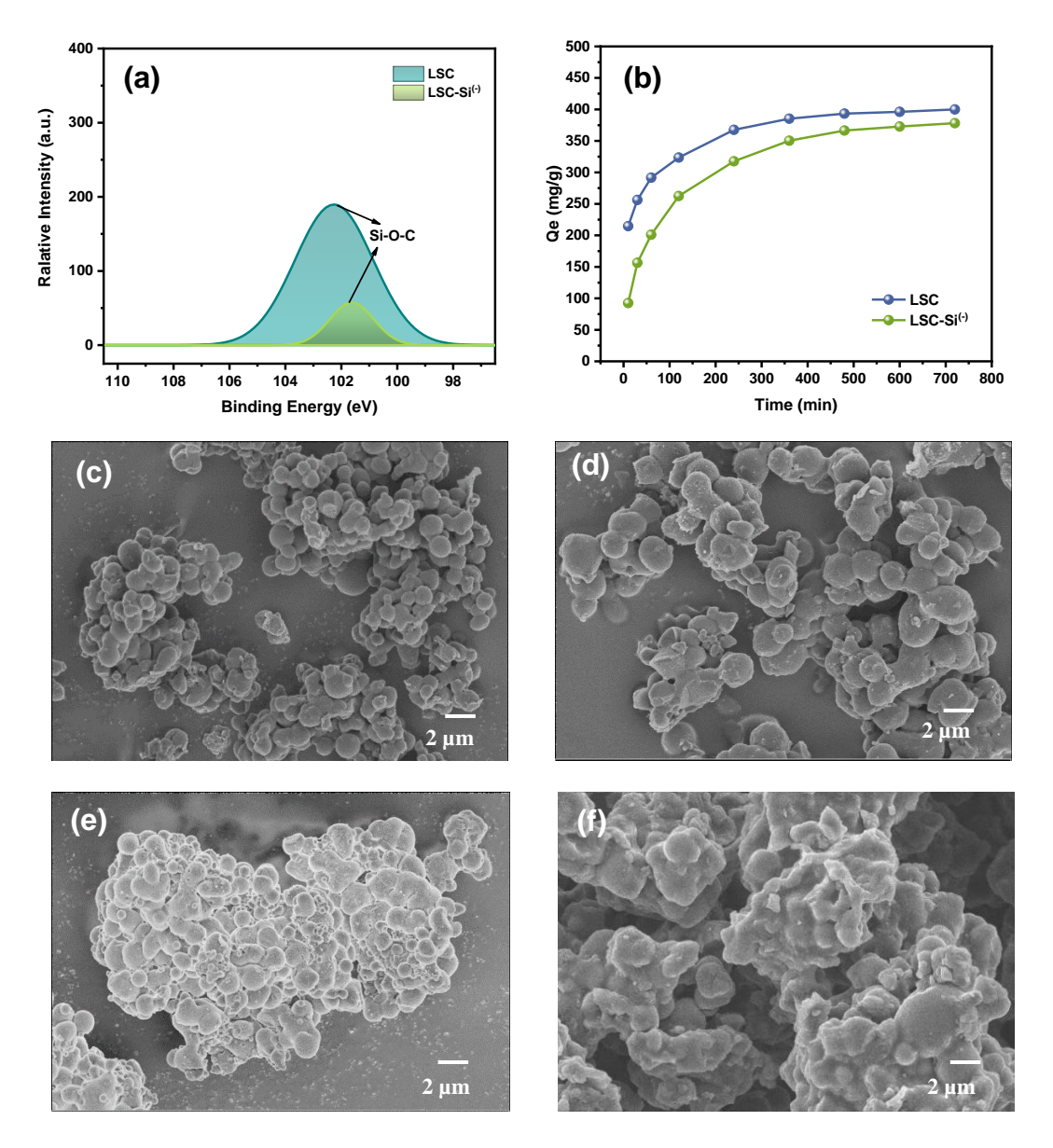


Fig. 1. LSC and LSC-Si⁽⁻⁾: (a) Si 2p spectra. (b) Comparison of adsorption rates for CIP. SEM image of LM(c), LSC (d), LM-Si⁽⁻⁾ (e) , LSC-Si⁽⁻⁾ (f)

Preparation of Lignin Spherical Activated Carbon Loaded with SiO₂

As shown in Fig. 2(a), the turbidity of both BL and BL with $10 \text{ g/L Na}_2\text{SiO}_3 \cdot 9\text{H}_2\text{O}$ (BL-Na₂SiO₃-10) exhibited an increasing and then decreasing trend during acid titration.

When the pH dropped below 7, the turbidity of BL-Na₂SiO₃-10 was significantly higher than that of BL, whereas the turbidity of the 10 g/L Na₂SiO₃·9H₂O solution remained relatively unchanged during titration. As depicted in Fig. 2(b), the presence of Si-O-Si bonds in LSC-Si⁽⁺⁾-10 indicated successful SiO₂ loading onto LSC. This suggests that the co-precipitation of SiO₂ and lignin occurred during acidification, coinciding with the pH reduction during titration. In the SiO₂ molecule, the oxygen atoms, possessing higher electronegativity than the silicon atoms, attract the surrounding hydrogen atoms. Consequently, hydrogen bonds form between SiO₂ and lignin molecules, leading to coprecipitation and the formation of lignin/ SiO₂ composites. According to the XRD image

in Fig. 2(c), LSC-Si⁽⁺⁾-10 exhibited an amorphous carbon structure along with an amorphous SiO₂ surface. As shown in Fig. 2(d), the adsorption amount on LSC-Si⁽⁺⁾-10 was significantly higher than that of LSC, indicating that SiO₂ loading on the surface of LSC enhanced its CIP adsorption capacity.

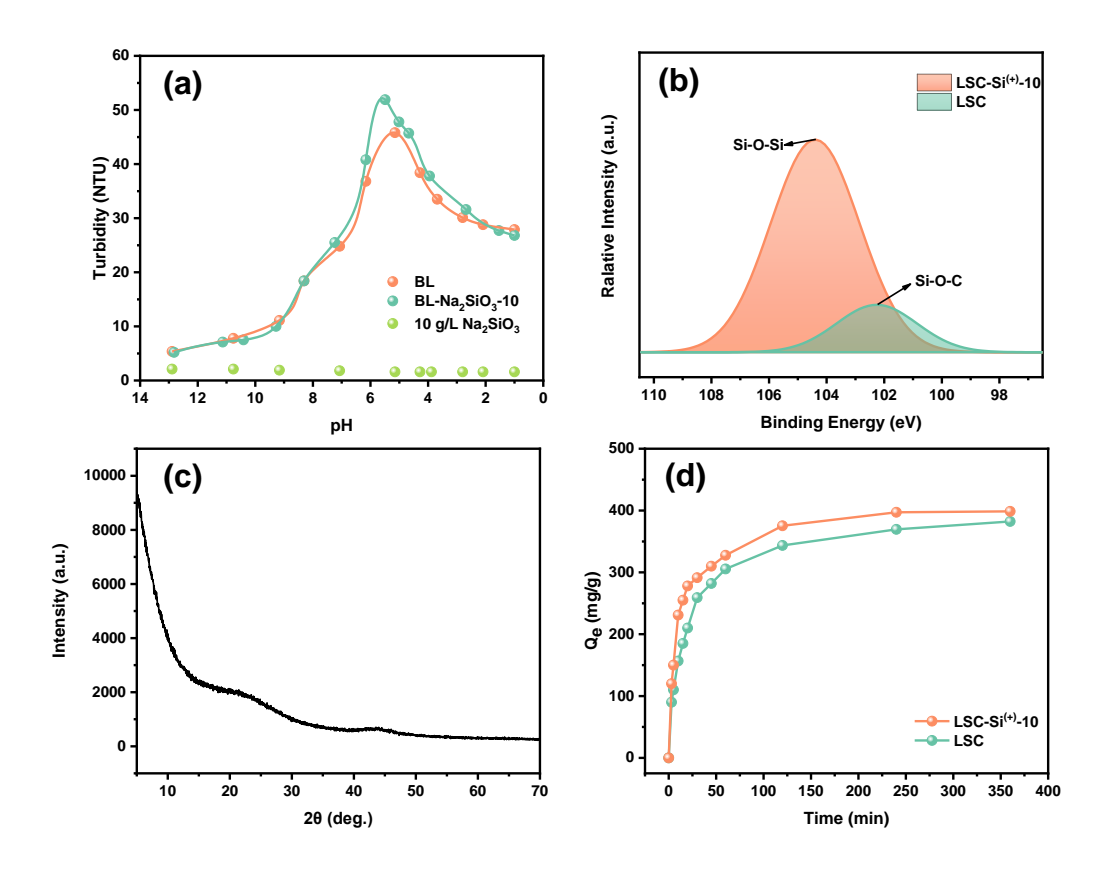


Fig. 2. (a) Turbidity curves of BL, BL-Na₂SiO₃-10 and 10 g/L Na₂SiO₃-9H₂O with pH, (b) Si 2p spectra of LSC-Si⁽⁺⁾-10 and LSC, (c) XRD pattern of LSC-Si⁽⁺⁾-10, (d) Comparison of adsorption capacities of LSC-Si⁽⁺⁾-10 and LSC

In summary, the incorporation of $Na_2SiO_3 \cdot 9H_2O$ successfully loaded SiO_2 onto LSC, enhancing its adsorption capacity for CIP. On the surface of LSC- $Si^{(+)}$ -10, Si-O-Si groups form numerous Si-O-Si bonds, and multiple groups contributed to a three-dimensional network structure through shared oxygen atoms. This structure significantly influences the material transport, pore structure, and surface chemistry of LSC- $Si^{(+)}$ -10, thereby enhancing the surface's activity and adsorption capacity.

Effect of Different Silica Contents on the Properties of LSC-Si⁽⁺⁾ FTIR and XPS

From the FTIR spectra shown in Fig. 3, the characteristic SiO₂ peaks of LM- Si⁽⁺⁾ (at 972 cm⁻¹) became more prominent with increasing Na₂SiO₃·9H₂O addition. Elemental analyses in Table 1 reveal that the Si and O content in LSC-Si⁽⁺⁾ increased with higher Na₂SiO₃·9H₂O additions, whereas the carbon content slightly decreased. However, carbon remained the dominant element, indicating that the hybrid materials, even with experimental Na₂SiO₃·9H₂O additions, are primarily lignin-carbon based. The Si content

in LSC-Si $^{(+)}$ -25 was notably higher, correlating with the concentration of Na₂SiO₃-9H₂O solution; a higher concentration results in more SiO₂ co-precipitated and loaded onto the lignin.

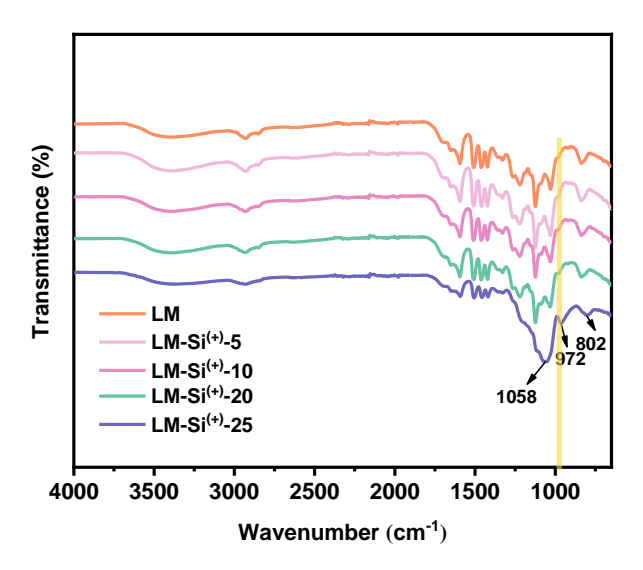


Fig. 3. FTIR spectroscopy of LM-Si⁽⁺⁾ with different SiO₂ content

Table 1. Elemental Analysis of LSC-Si⁽⁺⁾ with Different SiO₂ Content

Element	PP At. %								
	LSC-Si ⁽⁺⁾	LSC-Si ⁽⁺⁾ -5	LSC-Si ⁽⁺⁾ -10	LSC-Si ⁽⁺⁾ -20	LSC-Si ⁽⁺⁾ -25				
C 1s	93.17	87.91	81.37	76.36	55.04				
O 1s	4.87	8.78	10.09	12.24	19.18				
Si 2p	0.75	2.15	7.15	9.72	23.79				
N 1s	1.20	1.16	1.39	1.68	1.99				

SEM, BET, and adsorption of CIP

Comparing Figs. 4(a), (b), and (c) with Figs. 2(d) and (f), it becomes evident that with Na₂SiO₃·9H₂O additions of up to 20 g/L, the increased silicon content promoted the formation of a more regular and stable spherical structure in LSC, without noticeable collapse. This observation suggests that SiO₂ served as a stabilizer, preserving the spherical structure of lignin microspheres throughout the carbonization process. However, when Na₂SiO₃·9H₂O additions reached 25 g/L, excessive SiO₂ loading on the lignin surface hindered its ability to condense into a spherical structure during the hydrothermal reaction.

As illustrated in Figs. 5(a) and (b), with the increase of SiO₂ loading, the specific surface areas of LSC-Si⁽⁺⁾-5, LSC-Si⁽⁺⁾-10, and LSC-Si⁽⁺⁾-20 showed no significant change; however, their adsorption capacities for CIP significantly increased. Meantime, the specific surface area of LSC-Si⁽⁺⁾-25 decreased significantly, and its adsorption capacity significantly decreased. This indicates that pore adsorption was not the sole factor determining the CIP adsorption capacity of LSC. The presence of a moderate amount of SiO₂ can significantly enhance the adsorption capacity.

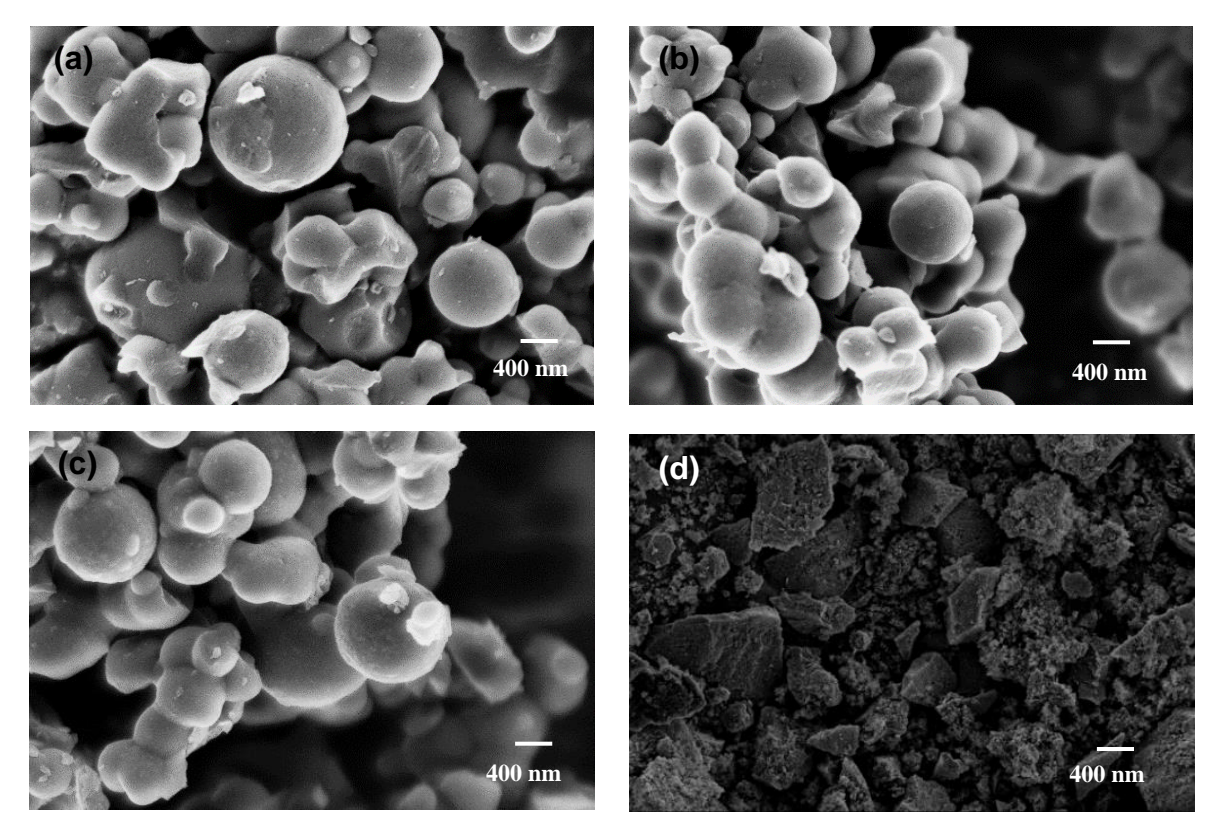


Fig. 4. SEM image of LSC-Si⁽⁺⁾-5 (a), LSC-Si⁽⁺⁾-10 (b), LSC-Si⁽⁺⁾-20 (c), LSC-Si⁽⁺⁾-25 (d)

To further verify the impact of SiO₂ on the adsorption capacity of CIP by LSC-Si⁽⁺⁾, the adsorption capacities of LSC-Si⁽⁺⁾ before and after desilication were compared (refer to Table S1 and Fig S1). These comparisons substantiate that the presence of a moderate amount of SiO₂ can significantly enhance the adsorption capacity. Given the morphology and adsorption capacity of the activated carbon, LSC-Si⁽⁺⁾-20 was selected for further investigation of its adsorption performance, with LSC serving as a comparison.

The adsorption capacities of LSC-Si⁽⁺⁾-20 and LSC for CIP, TC, and SDZ are displayed in Fig. 5(c). It is evident that the adsorption capacity of LSC-Si⁽⁺⁾-20 for the three antibiotics surpassed that of LSC. Furthermore, LSC-Si⁽⁺⁾-20 exhibited a higher adsorption capacity compared to other porous carbons (Jang *et al.* 2018; Canevesi *et al.* 2020; He *et al.* 2020; Meng *et al.* 2020; Geng *et al.* 2021). To further explore the adsorption characteristics of LSC-Si⁽⁺⁾-20, CIP was selected as the target adsorbent for a series of experiments.

The influence of pH on the adsorption activity of CIP by LSC-Si⁽⁺⁾-20 was explored. As indicated in Fig S1, the point of zero charge (pH_{pzc}) was found to be 7.5 for LSC and 6.5 for LSC-Si⁽⁺⁾-20. This reduction in pH_{pzc} for LSC-Si⁽⁺⁾-20, compared to LSC, is attributable to the surface loading of SiO₂, which has a pH_{pzc} of 2.5.

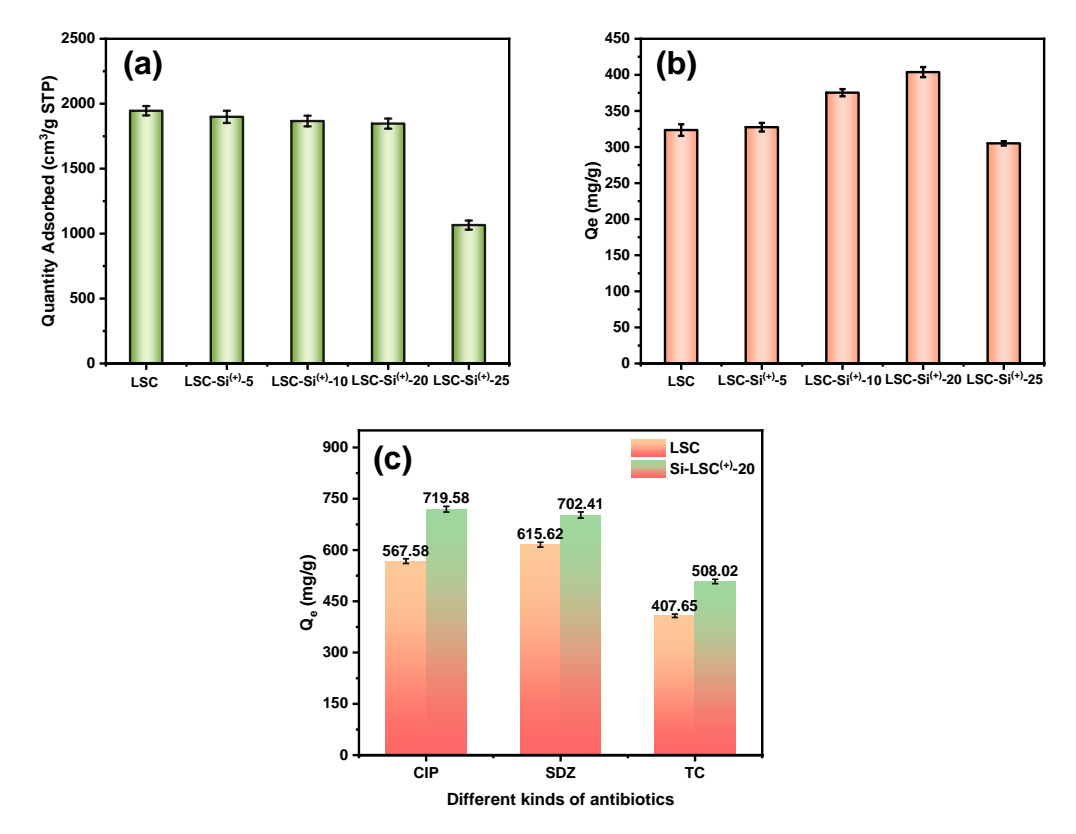


Fig. 5. Comparison of specific surface area (a) and CIP adsorption capacity (b) of porous carbon predesiliconization and after desilication, (c) Antibiotic diversity adsorption by LSC-Si⁽⁺⁾-20

Adsorption Capacity of LSC-Si⁽⁺⁾-20

Adsorption kinetics

Figure 6(a) presents the adsorption kinetics data. For LSC-Si⁽⁺⁾-20, the removal efficiency of CIP increased significantly within the first few min, reaching adsorption equilibrium after 60 min.

To elucidate the adsorption behavior of CIP on the adsorbent, the pseudo-primary kinetic model (PFOM), pseudo-secondary kinetic model (PSOM), and intra-particle diffusion model (IPDM) were employed to determine the controlling mechanisms of adsorption type and rate (Liu *et al.* 2022). The fitting results of these three models are displayed in Tables 2 and 3. Clearly, the PFOM (R² > 0.9659) and PSOM (R² > 0.9837) accurately described the adsorption behavior of CIP on LSC-Si⁽⁺⁾-20. Simultaneously, the experimental results are significant for PSOM, suggesting that CIP adsorption on the studied samples is predominantly driven by chemical processes (Meng *et al.* 2020; Wang *et al.* 2020).

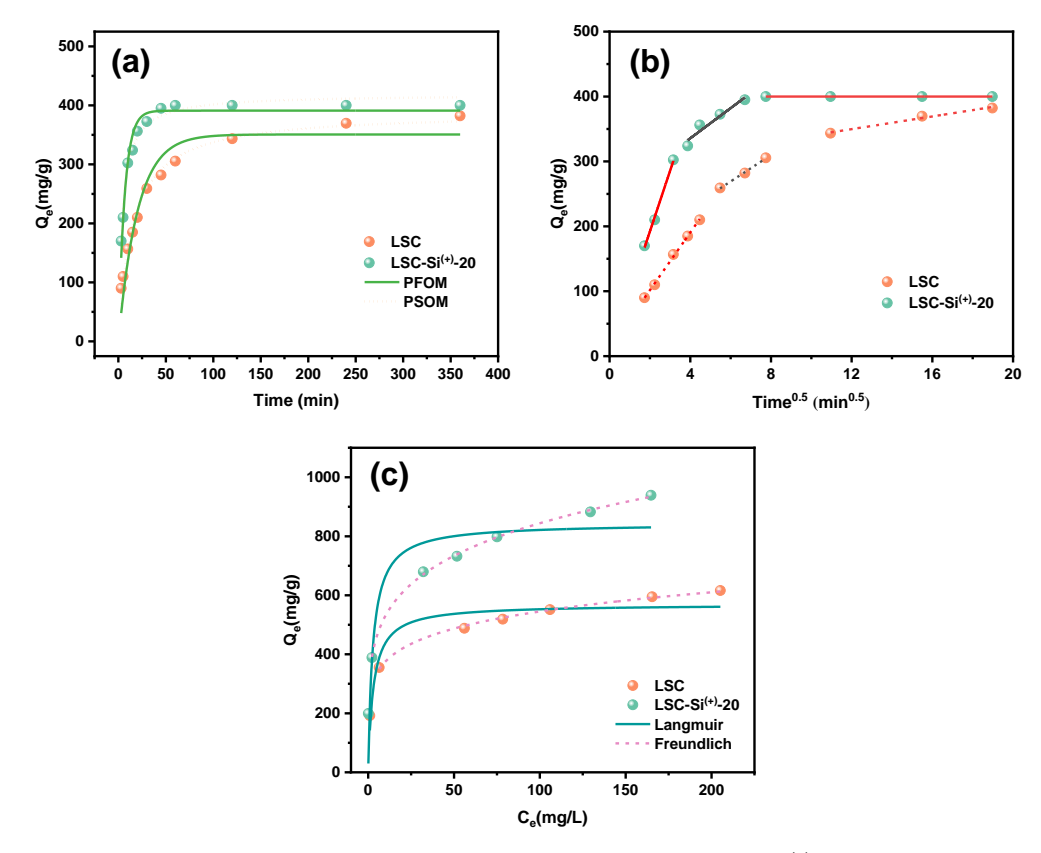


Fig. 6. Comparison of CIP adsorption properties of LSC and LSC-Si⁽⁺⁾-20, (a) influence of contact time and adsorption evaluation, (b) IPDM and (c) adsorption isotherm curves

Table 2. The Fitting Parameters of PFOM and PSOM of CIP Adsorption

	PFOM				PSOM	Q max, exp	
	Qe		R_1		K ₂	R^2	mg/g
	mg/g	1/h	κ-	mg/g	g/(mg· min)	κ-	
LSC	350.67	0.0491	0.9371	388.46	0.00017	0.9880	382.29
LSC-Si ⁽⁺⁾ -20	391.04	0.1499	0.9659	418.60	0.00056	0.9837	400.00

Table 3. The Fitting Parameters of IPDM of CIP Adsorption

	IPDM										
Adsorbents	Step 1			Step 2			Step 3				
	K _{1d}	C _{1d}	R ²	K _{2d}	C _{2d}	R^2	K _{3d}	C _{3d}	R^2		
LSC	44.38	12.95	0.9982	20.38	146.83	0.9966	4.88	291.23	0.9853		
LSC-Si ⁽⁺⁾ -20	93.44	5.28	0.9969	23.22	242.79	0.9303	0	400			

Continuous adsorption and desorption, as well as intraparticle diffusion are key steps in the adsorption (Hubbe *et al.* 2019). As illustrated in Fig. 6(b), due to the high concentration of CIP in the aqueous phase, the initial step involves the diffusion of CIP molecules to the surface of LSC-Si⁽⁺⁾-20 and subsequent occupation of active sites (Tian *et al.* 2023). The second step involves the dispersion of CIP molecules into the LSC-Si⁽⁺⁾-20

structure; as their concentration diminishes, adsorption eventually reaches equilibrium (Wu et al. 2016; Liu et al. 2017).

Adsorption isotherm

Analyzing the isotherm models of adsorbents is crucial, as it provides further insight into the interactions between the adsorbents and CIP. The adsorption isotherm data for CIP were nonlinearly fitted using the Langmuir and Freundlich models, with the results and model parameters displayed in Fig. 6(c) and Table. 4. The R^2 values for the isotherm models exceeded 0.95, suggesting that these models adequately characterize the adsorption process. For these adsorbents, the CIP adsorption process demonstrated monolayer chemisorption, characterized by homogeneous adsorption sites and significant electrostatic interactions, as evidenced by the higher R^2 values for the Langmuir model compared to the Freundlich model. Additionally, the Freundlich constant (1/n) being less than 1 indicates that the adsorption of CIP on these adsorbents was nonlinear and likely involves physical adsorption (Wang *et al.* 2020).

The viability of the adsorption process is effectively characterized by the equilibrium parameter (RL). LSC-Si⁽⁺⁾-20 and LSC exhibited favorable adsorption behavior, as indicated by their RL values (0.0082 and 0.0048, respectively), which fall within the 0 to 1.0 range (Xia *et al.* 2021). Under the experimental conditions, the maximum adsorption capacity (Q_{max}) for LSC-Si⁽⁺⁾-20 was recorded at 794 mg/g. Comparing the adsorption performance of other porous adsorbents for CIP (ranging from 10.4 to 600 mg/g), LSC-Si⁽⁺⁾-20 demonstrated a superior adsorption capacity for CIP (Peng *et al.* 2017; Zhang *et al.* 2017; Kong *et al.* 2020; Li *et al.* 2020; Wang *et al.* 2020; Velusamy *et al.* 2021; Atugoda *et al.* 2021; Ma 2021; Sayin *et al.* 2021; Theamwong *et al.* 2021; Tang *et al.* 2022; Wang *et al.* 2022).

Table 4. Adsorption Isothermal Parameters of LSC and LSC-Si⁽⁺⁾-20

Adsorbents	Langmuir				Freundlich			
	Qm	KL	R^2	R∟	K _F	1/n _F	R ²	Q _{max,exp} mg/g
	mg/g	L/mg	K-		mg/g			
LSC	605.12	2.3879	0.9972	0.0082	359.01	0.1070	0.9880	611.79
LSC-Si ⁽⁺⁾ -20	786.51	2.4067	0.9983	0.0048	428.73	0.1276	0.9686	793.61

Thermodynamics of the antibiotics adsorption behavior

The thermodynamic parameters derived from the equations are summarized in Table 5. The negative ΔG° values of CIP at 298, 308, and 318 K indicate the spontaneous and feasible nature of adsorption across these temperatures. As the temperature increased, the absolute value of ΔG° for LSC-Si⁽⁺⁾-20 also increased, suggesting that higher temperatures enhance antibiotic adsorption due to a greater driving force between the solution and solid phase (Zhang *et al.* 2015). The positive ΔH values suggest that the adsorption of target antibiotics is endothermic, aligning with the observed increase in adsorption at higher temperatures. The corresponding ΔS° values for LSC-Si⁽⁺⁾-20 were 359 kJ/(mol·K), indicating a reduction in the degree of freedom at the interface between the solid and solution phases upon adsorption of target antibiotics onto LSC-Si⁽⁺⁾-20 (Peng *et al.* 2015).

ΔG° (kJ/mol) Adsorbent ΔH° (kJ/mol) ΔS° (kJ/(mol·K)) 298 K 308 K 318 K LSC -6.92 -8.15 33.03 -9.60 133.93 LSC-Si(+)-20 -8.72 -12.03 -15.49 92.20 338.59

Table 5. Thermodynamic Parameters for the Adsorption of CIP onto LSC and LSC-Si⁽⁺⁾-20

Regeneration performance of LSC-Si⁽⁺⁾-20

Adsorption experiments involved mixing 10 mg of LSC-Si⁽⁺⁾-20 with 40 mL of an antibiotic solution at a concentration of 200 mg/L at 298 K. The mixture was oscillated at 298 K for 12 h to facilitate adsorption. Subsequently, the adsorbed porous carbon was heated to 700 °C at a rate of 10 °C/min under an N₂ atmosphere and pyrolyzed at this constant temperature for 60 min. Figure 7 illustrates that although the adsorption amount of CIP by LSC-Si⁽⁺⁾-20 decreased, it retained a high adsorption capacity after five cycles. In conclusion, LSC-Si⁽⁺⁾-20 demonstrates substantial regeneration capacity and offers economic advantages. This confirms that LSC-Si⁽⁺⁾-20 holds considerable potential for widespread application in antibiotic wastewater adsorption.

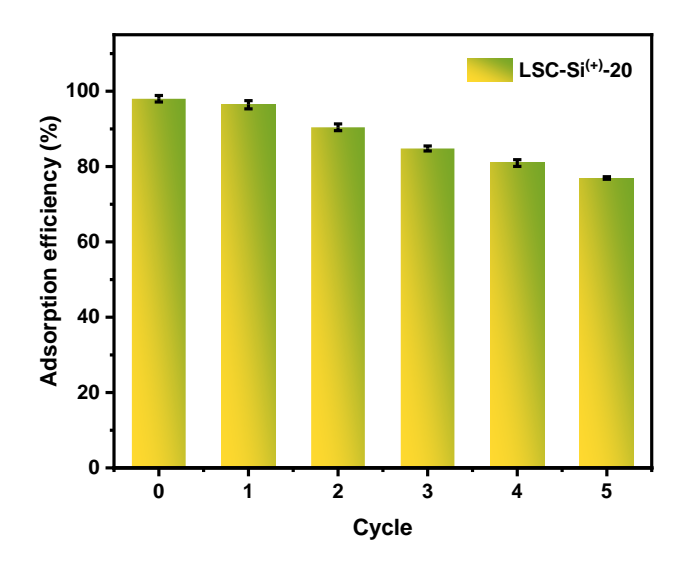


Fig. 7. Regeneration performance of CIP adsorption by LSC-Si⁽⁺⁾-20

Adsorption mechanism

Figure 8 depicts the potential mechanism of CIP adsorption by LSC-Si⁽⁺⁾-20. LSC-Si⁽⁺⁾-20, a heterogeneous adsorbent, which comprises LSC and SiO₂. LSC-Si⁽⁺⁾-20's high adsorption capacity for CIP is partly attributable to its large specific surface area (1846.74 m²/g) and the abundance of oxygen-containing functional groups that provide numerous favorable active sites (Wen *et al.* 2018). Additionally, it relates to the adsorption properties of the surface-loaded SiO₂. In solution, SiO₂ exhibits both hydrogen bonding and electrostatic adsorption with CIP. In aqueous solutions, the electrostatic interactions between LSC-Si⁽⁺⁾-20 and CIP effectively remove CIP, representing one of the adsorption mechanisms. Given the low solubility of the target antibiotic, the hydrophobic effect likely serves as the primary adsorption mechanism (Peng *et al.* 2015). The nitrogen atom in CIP's

piperazine group can be expected to form a hydrogen bond with the hydroxyl group of LSC-Si⁽⁺⁾-20 (Qiang *et al.* 2013). The delocalized π bond of the fluorine atom on CIP's benzene ring strongly retrieves electrons from the aryl ring, classifying it as a π -electron acceptor (Chen *et al.* 2015). Therefore, the adsorption process of CIP on LSC-Si⁽⁺⁾-20 may be facilitated by electrostatic interactions, hydrophobic effects, hydrogen bonding, and π - π interactions.

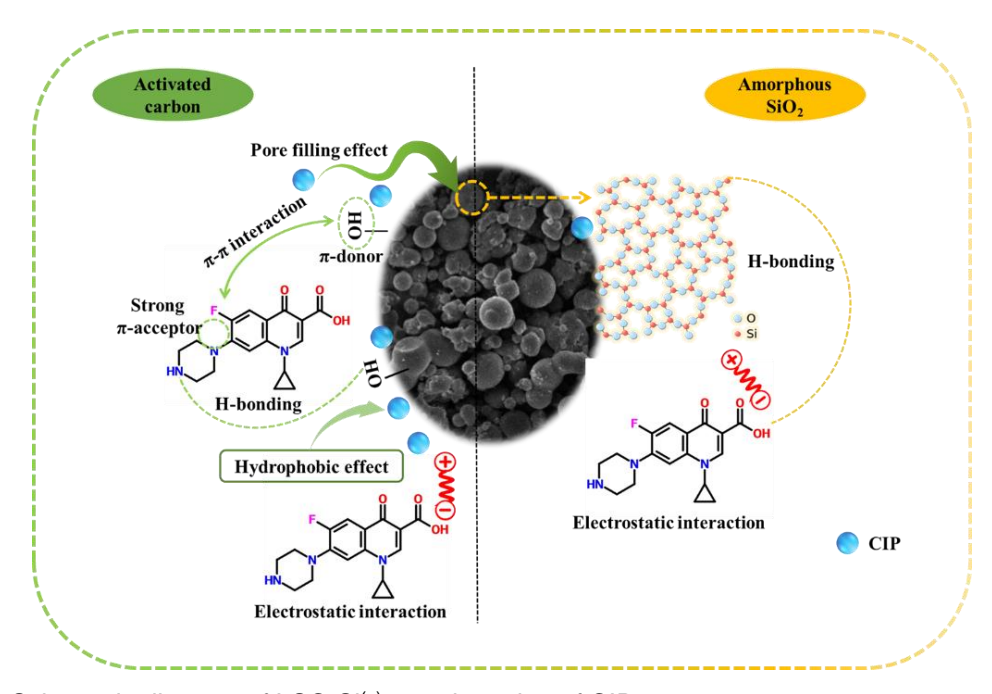


Fig. 8. Schematic diagram of LSC-Si(+)-20 adsorption of CIP

CONCLUSIONS

- 1. The presence of silicon enhances the adsorption capacity of lignin-based spherical carbon (LSC). Sodium silicate was added to the black liquor (BL), and SiO₂ was successfully loaded onto LSC through hydrogen-bonding co-precipitation with lignin under acidic conditions. SiO₂ serves as a stabilizer, maintaining the spherical structure of LSC and significantly enhancing its adsorption capacity.
- 2. A composite named LSC-Si⁽⁺⁾-20 demonstrated the best adsorption performance, with notable capacities for ciprofloxacin (CIP) (794 mg/g), tetracycline hydrochloride (TC) (508 mg/g), sulfadiazine (SDZ) (702 mg/g), and Cr⁶⁺ (406 mg/g).
- 3. LSC-Si⁽⁺⁾-20 possessed excellent physicochemical stability and good recyclability; it retained a high adsorption capacity after five cycles of recycling, offering new insights into addressing antibiotic pollution in water bodies.

ACKNOWLEDGMENTS

This research was funded by the National Natural Science Foundation of China (Grant 22206004).

REFERENCES CITED

- Al-Lagtah, N. M. A., Al-Muhtaseb, A. H., Ahmad, M. N. M., and Salameh, Y. (2016). "Chemical and physical characteristics of optimal synthesised activated carbons from grass-derived sulfonated lignin versus commercial activated carbons," *Microporous and Mesoporous Materials: The Offical Journal of the International Zeolite Association* 225, 504-514. DOI: 10.1016/j.micromeso.2016.01.043
- Atugoda, T., Gunawardane, C., Ahmad, M., and Vithanage, M. (2021). "Mechanistic interaction of ciprofloxacin on zeolite modified seaweed (*Sargassum crassifolium*) derived biochar: Kinetics, isotherm and thermodynamics," *Chemosphere* 281, article 130676. DOI: 10.1016/j.chemosphere.2021.130676
- Balandin, A. A. (2011). "Thermal properties of graphene and nanostructured carbon materials," *Nature Materials* 10, (8), 569-581. DOI: 10.1038/NMAT3064
- Ben, Y. B., Hu, M., Zhang, X. Y., Wu, S. M., Wong, M. H., Wang, M. Y., Andrews, C. B., and Zheng, C. M. (2020). "Efficient detection and assessment of human exposure to trace antibiotic residues in drinking water," *Water Research* 175, article 115699. DOI: 10.1016/j.watres.2020.115699
- Canevesi, R. L. S., Sanchez-Sanchez, A., Gadonneix, P., Celzard, A., and Fierro, V. (2020). "Hierarchical tannin-derived carbons as efficient tetracycline adsorbents," Applied Surface Science 533, article 147428. DOI: 10.1016/j.apsusc.2020.147428
- Cha, Y. L., Alam, A. M., Park, S. M., Moon, Y. H., Kim, K. S., Lee, J. E., Kwon, D. E., and Kang, Y. G. (2020). "Hydrothermal-process-based direct extraction of polydisperse lignin microspheres from black liquor and their physicochemical characterization," *Bioresource Technology* 297, article 122399. DOI: 10.1016/j.biortech.2019.122399
- Chen, W. R., Li, X. K., Pan, Z. Q., Bao, Y. X., Ma, S. S., and Li, L. S. (2015). "Efficient adsorption of Norfloxacin by Fe-MCM-41 molecular sieves: Kinetic, isotherm and thermodynamic studies," *Chemical Engineering Journal* 281, 397-403. DOI: 10.1016/j.cei.2015.06.121
- Fan, L. P. (2020). "Hydrothermal synthesis of lignin-based carbon microspheres as anode material for lithium-ion batteries," *International Journal of Electrochemical Science* 15, (2), 1035-1043. DOI: 10.20964/2020.02.16
- Fan, L. L., Shi, Z. Q., Ren, Q. J., Yan, L., Zhang, F. M., and Fan, L. P. (2020). "Nitrogen-doped lignin based carbon microspheres as anode material for high performance sodium ion batteries," *Green Energy & Environment* 2, 220-228. DOI: 10.1016/j.gee.2020.06.005
- Gao, Y., Li, Y. Z., Liang, C., Cen, P. P., Xi, J., Guo, Y., Song, W. M., and Liu, X. Y. (2021). "Two mesoporous anionic metal—organic frameworks for selective and efficient adsorption of a cationic organic dye," *Dalton Transactions* 50, (47), 17603-17610. DOI: 10.1039/D1DT03131G
- Geng, X. X., Lv, S. Y., Yang, J., Cui, S. H., and Zhao, Z. H. (2021). "Carboxyl-functionalized biochar derived from walnut shells with enhanced aqueous adsorption of sulfonamide antibiotics," *Journal of Environmental Management* 280, artcle 111749. DOI: 10.1016/j.jenvman.2020.111749
- Goldstein, M., Shenker, M., and Chefetz, B. (2014). "Insights into the uptake processes of wastewater-borne pharmaceuticals by vegetables," *Environmental Science & Technology* 48, (10), 5593-5600. DOI: 10.1021/es5008615
- Guo, N. N., Li, M., Sun, X. K., Wang, F., and Yang, R. (2017). "Enzymatic hydrolysis

- lignin derived hierarchical porous carbon for supercapacitors in ionic liquids with high power and energy densities," *Green Chemistry* 19(11), 2595-2602. DOI: 10.1039/C7GC00506G
- Han, S. J., Sohn, K., and Hyeon, T. (2000). "Fabrication of new nanoporous carbons through silica templates and their application to the adsorption of bulky dyes," *Chemistry of Materials* 12, (11), 3337-3341. DOI: 10.1021/cm000106t
- He, X. L., Li, J. L., Meng, Q. M., Guo, Z. Y., Zhang, H., and Liu, Y. R. (2020). "Enhanced adsorption capacity of sulfadiazine on tea waste biochar from aqueous solutions by the two-step sintering method without corrosive activator," *Journal of Environmental Chemical Engineering* 9(1), article 104898. DOI: 10.1016/j.jece.2020.104898
- Ho, H. C., Bonnesen, P. V., Nguyen, N. A., Cullen, D. A., Uhrig, D., Goswami, M., Keum, J. K., and Naskar, A. K. (2019). "Method to synthesize micronized spherical carbon particles from lignin," *Industrial & Engineering Chemistry Research* 59(1), 9-17. DOI: 10.1021/acs.iecr.9b05143
- Hou, Y. R., Liang, Y., Hu, H. B., Tao, Y. P., Zhou, J. C., and Cai, J. J. (2021). "Facile preparation of multi-porous biochar from lotus biomass for methyl orange removal: Kinetics, isotherms, and regeneration studies," *Bioresource Technology* 329(39), article 124877. DOI: 10.1016/j.biortech.2021.124877
- Huang, W., Chen, J., and Zhang, J. Q. (2018). "Adsorption characteristics of methylene blue by biochar prepared using sheep, rabbit and pig manure," *Environmental Science and Pollution Research International* 25, 29256-29266. DOI: 10.1007/s11356-018-2906-1
- Hubbe, M. A., Azizian, S., and Douven, S. (2019). "Implications of apparent pseudo-second-order adsorption kinetics onto cellulosic materials. A review," *BioResources* 14(3), 7582-7626. DOI: 10.15376/biores.14.3.7582-7626
- Jang, H. M., Yoo, S., Choi, Y. K., Park, S., and Kan, E. (2018). "Adsorption isotherm, kinetic modeling and mechanism of tetracycline on *Pinus taeda*-derived activated biochar," *Bioresource Technology* 259, 24-31. DOI: 10.1016/j.biortech.2018.03.013
- Jiang, G. J. (2019). "Preparation and electrochemical properties of lignin porous carbon spheres as the negative electrode of lithium ion batteries," *International Journal of Electrochemical Science* 14(6), 5422-5434. DOI: 10.20964/2019.06.36
- Kameda, T., Horikoshi, K., Kumagai, S., Saito, Y., and Yoshioka, T. (2020). "Adsorption of urea, creatinine, and uric acid from three solution types using spherical activated carbon and its recyclability," *Chinese Journal of Chemical Engineering* 28(12), 2993-3001. DOI: 10.1016/j.cjche.2020.03.018
- Kong, J. J., Zheng, Y. J., Xiao, L. J., Dai, B. L., Meng, Y. J., Ma, Z. Y., Wang, J. H., and Huang, X. C. (2020). "Synthesis and comparison studies of activated carbons based folium cycas for ciprofloxacin adsorption," *Colloids and Surfaces A: Physicochemical and Engineering Aspects* 606, article 125519. DOI: 10.1016/j.colsurfa.2020.125519
- Li, J., Pan, L. J., Yu, G. W., Li, C. X., Xie, S. Y., and Wang, Y. (2020). "Synthesis of an easily recyclable and safe adsorbent from sludge pyrochar for ciprofloxacin adsorption," *Environmental Research* 192, article 110258. DOI: 10.1016/j.envres.2020.110258
- Lima E. C., Hosseini-Bandegharaei A., Moreno-Piraján J. C., and Anastopoulos I. (2019). "A critical review of the estimation of the thermodynamic parameters on adsorption equilibria. Wrong use of equilibrium constant in the Van't Hoof equation

- for calculation of thermodynamic parameters of adsorption," *Journal of Molecular Liquids* 273, 425-434. DOI:10.1016/j.molliq.2018.10.048
- Liu, J., Wickramaratne, N. P., Qiao, S. Z., and Jaroniec, M. (2015). "Molecular-based design and emerging applications of nanoporous carbon spheres," *Nature Materials* 14, (8), 763-774. DOI: 10.1038/nmat4317
- Liu, P. P., Wang, Q. R., Zheng, C. L., and He, C. (2017). "Sorption of sulfadiazine, norfloxacin, metronidazole, and tetracycline by granular activated carbon: Kinetics, mechanisms, and isotherms," *Water, Air and Soil Pollution* 228(4), article 129. DOI: 10.1007/s11270-017-3320-x
- Liu, S., Wei, W. G., Wu, S. B., and Zhang, F. S. (2020). "Preparation of hierarchical porous activated carbons from different industrial lignin for highly efficient adsorption performance," *Journal of Porous Materials* 27, (5), 1523-1533. DOI: 10.1007/s10934-020-00926-9
- Liu, Y. J., Guo, H., Zhang, B. H., Wen, G. Y., Vajtai, R., Wu, L., Ajayan, P. M., and Wang, L. (2020). "Sustainable synthesis of N-doped hollow porous carbon spheres via a spray-drying method for lithium-sulfur storage with ultralong cycle life," *Batteries & Supercaps* (11), 1201-1208. DOI: 10.1002/batt.202000143
- López-Serna, R., Jurado, A., Vázquez-Suñé, E., Carrera, J., Petrovic, M., and Barceló, D. (2013). "Occurrence of 95 pharmaceuticals and transformation products in urban groundwaters underlying the metropolis of Barcelona, Spain," *Environmental Pollution* 174*C*, 305-315. DOI: 10.1016/j.envpol.2012.11.022
- Ma, J., Yu, F., Zhou, L., Jin, L., Yang, M. X., Luan, J. S., Tang, Y. H., Fan, H. B., Yuan, Z. W., and Chen, J. H. (2012). "Enhanced adsorptive removal of methyl orange and methylene blue from aqueous solution by alkali-activated multiwalled carbon nanotubes," *ACS Appl Mater Interfaces* 4(11), 5749-5760. DOI: 10.1021/am301053m
- Ma, Y. F., Li, M., Li, P., Yang, L., Wu, L., Gao, F., Qi, X. B., and Zhang, Z. L. (2021). "Hydrothermal synthesis of magnetic sludge biochar for tetracycline and ciprofloxacin adsorptive removal," *Bioresource Technology* 319(1), article 124199. DOI: 10.1016/j.biortech.2020.124199
- Mao, H. Y., Chen, X. W., Huang, R. Z., Chen, M. Z., Yang, R., Lan, P., Zhou, M. J., Zhang, F., Yang, Y., and Zhou, X. Y. (2018). "Fast preparation of carbon spheres from enzymatic hydrolysis lignin: Effects of hydrothermal carbonization conditions," *Scientific Reports* 8(1), article 9501. DOI: 10.1038/s41598-018-27777-4
- Meng, Q. M., Zhang, Y. L., Meng, D., Liu, X. ., Zhang, Z. J., Gao, P. L., Lin, A. G., and Hou, L. (2020). "Removal of sulfadiazine from aqueous solution by in-situ activated biochar derived from cotton shell," *Environmental Research* 191(5), article 110104. DOI: 10.1016/j.envres.2020.110104
- Moreno, A., and Sipponen, M. H. (2020). "Lignin-based smart materials: a roadmap to processing and synthesis for current and future applications," *Materials Horizons* 9, 2237-2257. DOI: 10.1039/D0MH00798F
- Munoz, M., Kolb, V., Lamolda, A., de Pedro, Z. M., Modrow, A., Etzold, B. J. M., Rodriguez, J. J., and Casas, J. A. (2017). "Polymer-based spherical activated carbon as catalytic support for hydrodechlorination reactions," *Applied Catalysis B Environmental An International Journal Devoted to Catalytic Science & Its Applications* 218, 498-505. DOI: 10.1016/j.apcatb.2017.07.001
- Ouzzine, M., Romero-Anaya, A. J., Lillo-Ródenas, M. A., and Linares-Solano, A. (2019). "Spherical activated carbons for the adsorption of a real multicomponent VOC mixture," *Carbon* 148, 214-223. DOI: 10.1016/j.carbon.2019.03.075

- Pang, T. R., Wang, G. H., Ge, J., Wei, N., Sui, W. J., Parvez, A. M., and Si, C. L. (2021). "Novel surfactant-assisted hydrothermal fabrication of a lignin microsphere as a green reducer and carrier for Pd nanoparticles," *ACS Sustainable Chemistry & Engineering* 9(50), 17085-17095. DOI: 10.1021/acssuschemeng.1c06170
- Peng, X. M., Hu, F. P., Lam, F. L. Y., Wang, Y. J., Liu, Z. M., and Dai, H. L. (2015). "Adsorption behavior and mechanisms of ciprofloxacin from aqueous solution by ordered mesoporous carbon and bamboo-based carbon," *Journal of Colloid and Interface Science* 460, 349-360. DOI: 10.1016/j.jcis.2015.08.050
- Peng, X. M., Hu, F. P., Zhang, T., Qiu, F. X., and Dai, H. L. (2017). "Amine-functionalized magnetic bamboo-based activated carbon adsorptive removal of ciprofloxacin and norfloxacin: A batch and fixed-bed column study," *Bioresource Technol.* 249, 924-934. DOI: 10.1016/j.biortech.2017.10.095.
- Qiang, Z. M., Bao, X. L., and Ben, W. W. (2013). "MCM-48 modified magnetic mesoporous nanocomposite as an attractive adsorbent for the removal of sulfamethazine from water," *Water Research* 47(12), 4107-4114. DOI: 10.1016/j.watres.2012.10.039.
- Qiu, W. H., Sun, J., Fang, M. J., Luo, S. S., Tian, Y. Q., Dong, P. Y., Xu, B. T., and Zheng, C. M. (2019). "Occurrence of antibiotics in the main rivers of Shenzhen, China: Association with antibiotic resistance genes and microbial community," *Science of The Total Environment* 653(Feb. 25), 334-341. DOI: 10.1016/j.scitotenv.2018.10.398.
- Reichel, R., Michelini, L., Ghisi, R., and Thiele-Bruhn, S. (2015). "Soil bacterial community response to sulfadiazine in the soil—root zone," *Journal of Plant Nutrition and Soil Science* 178(3), 499-506. DOI: 10.1002/jpln.201400352.
- Sayin, F., Akar, S. T., and Akar, T. (2021). "From green biowaste to water treatment applications: Utilization of modified new biochar for the efficient removal of ciprofloxacin," *Sustainable Chemistry and Pharmacy* 24, article 100522. DOI: 10.1016/j.scp.2021.100522
- Sophia, A. C., and Lima, E. C. (2018). "Removal of emerging contaminants from the environment by adsorption," *Ecotoxicology and Environmental Safety* 150, 1-17. DOI: 10.1016/j.ecoenv.2017.12.026
- Sun, X. M., and Li, Y. D. (2004). "Colloidal carbon spheres and their core/shell structures with noble-metal nanoparticles," *Angewandte Chemie-International Edition* 43(5), 597-601. DOI: 10.1002/anie.200352386
- Tang, Y. H., Hao, J. J., He, S. X., Luo, T. T., Wu, L.S., Wang, X. T., and Guo, J. Q. (2022). "Characterization of edible fungus substrate modified biochar and its adsorption capacity for ciprofloxacin hydrochloride," *Bulletin of Environmental Contamination and Toxicology* 108(6), 1153-1158. DOI:10.1007/s00128-022-03463-0
- Theamwong, N., Intarabumrung, W., Sangon, S., Aintharabunya, S., Ngernyen, Y., Hunt, A. J., and Supanchaiyamat, N. (2021). "Activated carbons from waste *Cassia bakeriana* seed pods as high-performance adsorbents for toxic anionic dye and ciprofloxacin antibiotic remediation," *Bioresource Technology* 341, article 125832. DOI: 10.1016/j.biortech.2021.125832
- Thiele-Bruhn, S., and Beck, I. C. (2005). "Effects of sulfonamide and tetracycline antibiotics on soil microbial activity and microbial biomass," *Chemosphere* 59(4), 457-465. DOI: 10.1016/j.chemosphere.2005.01.023
- Tian, Y. J., Zhu, J. Y., Ying, C. H., Luo, H. W., Zhang, S. F., Zhang, L. Q., Li, R. N., and Li, J. (2023). "Photoaging processes of polyvinyl chloride microplastics enhance the

- adsorption of tetracycline and facilitate the formation of antibiotic resistance," *Chemosphere* 320, article 13820. DOI: 10.1016/j.chemosphere.2023.137820
- Tran, H. N., Tomul, F., Ha, N. T. H., Nguyen, D. T., Lima, E. C., Le, G. T., Chang, C. T., Masindi, V., and Woo, S. H. (2020). "Innovative spherical biochar for pharmaceutical removal from water: Insight into adsorption mechanism," *Journal of Hazardous Materials* 394, article 122255. DOI: 10.1016/j.jhazmat.2020.122255
- Valetti, S., Feiler, A., and Trulsson, M. (2017). "Bare and effective charge of mesoporous silica particles," *Langmuir* 33, (29), 7343-7351. DOI: 10.1021/acs.langmuir.7b01135
- Valetti, S., Adam, F., and Martin T. S. (2017). "Bare and effective charge of mesoporous silica particles," *Langmuir* 33(29), 7343-7351. DOI: 10.1016/j.jclepro.2021.128283
- Velusamy, K., Periyasamy, S., Kumar, P. S., Jayaraj T., Krishnasamy R., Sindhu J., Sneka D., Subhashini B., and Vo D. N. (2021). "Analysis on the removal of emerging contaminant from aqueous solution using biochar derived from soap nut seeds," *Environmental Pollution* 287, article 117632. DOI: 10.1016/j.envpol.2021.117632
- Wang, B., Mo, Q. Y., Qin, B., Song, L., Li, J., Sheng, G. S., Shi, D. Z., Xu, X. Y., and Hou, L. A. (2022). "Adsorption behaviors of three antibiotics in single and coexisting aqueous solutions using mesoporous carbon," *Environmental Research* 215, article 114375. DOI: 10.1016/j.envres.2022.114375
- Wang, B., Xu, X. Y., Tang, H., Mao, Y. L., Chen, H. H., and Ji, F. Y. (2020). "Highly efficient adsorption of three antibiotics from aqueous solutions using glucose-based mesoporous carbon," *Applied Surface Science* 528, article 147048. DOI: 10.1016/j.apsusc.2020.147048
- Wang, H. B., Cai, J. Y., Liao, Z. W., Jawad, A., Ifthikar, J., Chen, Z. L., and Chen, Z. Q. (2020). "Black liquor as biomass feedstock to prepare zero-valent iron embedded biochar with red mud for Cr(VI) removal: Mechanisms insights and engineering practicality," *Bioresource Technology* 311, article 123553. DOI: 10.1016/j.biortech.2020.123553
- Wang, H. R., Zhou, H. W., Gao, M., Zhu, Y. A., Liu, H. T., Gao, L., and Wu, M. X. (2019). "Hollow carbon spheres with artificial surface openings as highly effective supercapacitor electrodes," *Electrochimica Acta* 298, 552-560. DOI: 10.1016/j.electacta.2018.12.070
- Wang, T., Okejiri, F., Qiao, Z. A., and Dai, S. (2020). "Tailoring polymer colloids derived porous carbon spheres based on specific chemical reactions," *Advanced Materials* 32(44), article 2002475. DOI: 10.1002/adma.202002475
- Wang, T., Zhong, Y., Wang, C., and Tong, G. (2021). "A low capital method for silicon interference in bamboo kraft pulping alkaline recovery system," *J. Clean Prod.* 11, article 128283. DOI: 10.1016/j.jclepro.2021.128283
- Xia, S. M., Deng, L., Liu, X., Yang, L. F., Yang, X. Z., Shi, Z., and Pei, Y. (2021). "Fabrication of magnetic nickel incorporated carbon nanofibers for superfast adsorption of sulfadiazine: Performance and mechanisms exploration," *Journal of Hazardous Materials* 423(Pt B), article 127219. DOI: 10.1016/j.jhazmat.2021.127219
- Xu, F., Lu, Q. W., Li, K. P., Zhu, T. T., Wang, W. K., and Hu, Z. H. (2020). "Green synthesis of magnetic mesoporous carbon from waste-lignin and its application as an efficient heterogeneous Fenton catalyst," *Journal of Cleaner Production* 285(12), article 125363. DOI: 10.1016/j.jclepro.2020.125363
- Yu, B. J., Chang, Z. Z., Zhang, Y., and Wang, C. Y. (2018). "Preparation and formation mechanism of size-controlled lignin based microsphere by reverse phase polymerization," *Materials Chemistry and Physics* 203, 97-105. DOI:

- 10.1016/j.matchemphys.2017.08.039
- Zhang, B. P., Han, X. L., Gu, P. J., Fang, S. Q., and Bai, J. (2017). "Response surface methodology approach for optimization of ciprofloxacin adsorption using activated carbon derived from the residue of desilicated rice husk," *Journal of Molecular Liquids* 238, 316-325. DOI: 10.1016/j.molliq.2017.04.022
- Zhang, C., Xue, J. M., Cheng, D. M., Feng, Y., Liu, Y. W., Aly, H. M., and Li, Z. J. (2019). "Uptake, translocation and distribution of three veterinary antibiotics in *Zea mays* L," *Environmental Pollution* 250(Jul.), 47-57. DOI: 10.1016/j.envpol.2019.03.110
- Zhang, D., Cui, K., Wang, T. T., Dong, H. Y., Feng, W. Y., Ma, C., and Dong, Y. L. (2018). "Trends in and correlations between antibiotic consumption and resistance of *Staphylococcus aureus* at a tertiary hospital in China before and after introduction of an antimicrobial stewardship programme," *Epidemiology and Infection* 147, article e48, 1-6. DOI: 10.1017/S0950268818003059
- Zhang, G. X., Liu, X. T., Sun, K., He, Q. S., Qian, T. W., and Yan, Y. L. (2013). "Interactions of simazine, metsulfuron-methyl, and tetracycline with biochars and soil as a function of molecular structure," *Journal of Soils&Sediments* 13, 1600-1610. DOI: 10.1007/s11368-013-0755-6
- Zhang, Z. Y., Lan, H. C., Liu, H. J., and Qu, J. H. . (2015). "Removal of tetracycline antibiotics from aqueous solution by amino-Fe (III) functionalized SBA15," *Colloids & Surfaces A Physicochemical & Engineering Aspects* 471, 133-138. DOI: 10.1016/j.colsurfa.2015.02.018
- Zhao, H. J., Wang, Q. J., Deng, Y. H., Shi, Q., Qian, Y., Wang, B. B., Lü, L., and Qiu, X. Q. (2016). "Preparation of renewable lignin-derived nitrogen-doped carbon nanospheres as anodes for lithium-ion batteries," *RSC Advances* 6(81), 77143-77150. DOI: 10.1039/C6RA17793J
- Zhong, R. S., Yang D. J., Xiong, W. L., Guo W. Y., and Qiu, X. Q. (2015). "Preparation of lignin-based silica composite nanoparticles and its application in HDPE," *CIESC Journal* 66(08), 3255-3261. DOI: 10.11949/j.issn.0438-1157.20150636
- Zhou, X., and Zhou, X. (2014). "The unit problem in the thermodynamic calculation of adsorption using the langmuir equation," *Chemical Engineering Communications* 201(11), 1459-1467. DOI: 10.1080/00986445.2013.818541

Article submitted: Dec. 24, 2024; Peer review completed: Feb. 1, 2025; Revised version received: Feb. 26, 2025; Accepted: April 1, 2025; Published: April 18, 2025. DOI: 10.15376/biores.20.2.4229-4249